Baryon emission at target rapidities in Si+Al,Cu,Au collisions at 14.6*A* GeV/*c* and Au+Au collisions at 11.7*A* GeV/*c*

L. Ahle,[10] Y. Akiba,[6] D. Beavis,[2] P. Beery,[4] H. C. Britt,[9] B. Budick,[11] C. Chasman,[2] Z. Chen,[2] C. Y. Chi,[5] Y. Y. Chu,[2] V. Cianciolo,[10,*] B. A. Cole,[5,†] J. B. Costales,[9,‡] H. J. Crawford,[3] J. B. Cumming,[2] R. Debbe,[2] J. Engelage,[3] S. Y. Fung,[4] M. Gonin,[2,§] S. Gushue,[2] H. Hamagaki,[6] R. S. Hayano,[12] S. Hayashi,[2] S. Homma,[6] H. Kaneko,[7] J. Kang,[14] S. Kaufman,[1] W. L. Kehoe,[10] K. Kurita,[13,‖] R. J. Ledoux,[10,‡] M. J. LeVine,[2] Y. Miake,[13] D. P. Morrison,[10,¶] R. J. Morse,[10,**] B. Moskowitz,[2] S. Nagamiya,[5] M. N. Namboodiri,[9] T. K. Nayak,[5,††] J. Olness,[2] C. G. Parsons,[10,‡‡] L. P. Remsberg,[2] D. Roerich,[2,§§] P. Rothschild,[10] H. Sakurai,[12] T. C. Sangster,[9] R. Seto,[4] K. Shigaki,[12] R. Soltz,[10,*] P. Stankus,[5,‖‖] S. G. Steadman,[10] G. S. F. Stephans,[10] T. Sung,[10] Y. Tanaka,[8] M. J. Tannenbaum,[2] J. Thomas,[9] S. Tonse,[9] S. Ueno,[13] J. H. van Dijk,[2] F. Videbaek,[2] O. Vossnack,[5,††] V. Vustadakis,[10] F. Q. Wang,[5] Y. Wang,[5] H. E. Wegner,[2,12,¶¶] D. S. Woodruff,[9] Y. D. Wu,[5] K. Yagi,[13] X. Yang,[5] D. Zachary,[10] and W. A. Zajc[5]
(E802 Collaboration)

[1]*Argonne National Laboratory, Argonne, Illinois 60439*
[2]*Brookhaven National Laboratory, Upton, New York 11973*
[3]*University of California, Space Sciences Laboratory, Berkeley, California 94720*
[4]*University of California, Riverside, California 92507*
[5]*Columbia University, New York, New York 10027 and Nevis Laboratories, Irvington, New York 10533*
[6]*Institute for Nuclear Study, University of Tokyo, Tokyo 188, Japan*
[7]*Kyoto University, Sakyo-Ku, Kyoto 606, Japan*
[8]*Kyushu University, Fukuoka 812, Japan*
[9]*Lawrence Livermore National Laboratory, Livermore, California 94550*
[10]*Massachusetts Institute of Technology, Cambridge, Massachusetts 02139*
[11]*New York University, New York, New York 10003*
[12]*Department of Physics, University of Tokyo, Tokyo 113, Japan*
[13]*University of Tsukuba, Tsukuba, Ibaraki 305, Japan*
[14]*Yonsei University, Seoul 120-749, Korea*

(Received 19 June 1996; revised manuscript received 30 January 1997)

We report measurements of proton emission at target rapidities for minimum bias and central collisions of 14.6*A* GeV/*c* ^{28}Si with Al, Cu, and Au nuclei as well as minimum bias and central collisions of 11.7*A* GeV/*c* ^{197}Au with Au nuclei. Results for deuteron emission are also reported for the Si+Au reaction. The spectra span the laboratory angular range of $50° \leqslant \theta \leqslant 130°$ and kinetic energy range of $40\ \mathrm{MeV} \leqslant E_{\mathrm{kin}} \leqslant 225\ \mathrm{MeV}$. Inverse slopes of proton spectra and proton $dN/d\eta$ values in the kinetic energy range $50\ \mathrm{MeV} \leqslant E_{\mathrm{kin}} \leqslant 110\ \mathrm{MeV}$ are reported. The inverse slopes are 40–80 MeV for the various systems, generally increasing with increasing pseudorapidity. The $dN/d\eta$ values for $A+A$ collisions within the restricted kinetic energy interval are compared to those for protons from $p+\mathrm{Au}$ in the literature. All pseudorapidity distributions have very similar shapes. The experimental results have been compared to the predictions of the nucleon-nucleon collision models ARC and RQMD. The predictions made by these two models for the distribution of protons at target rapidities are very similar to each other. However, there are significant differences between the model predictions and the experimental results in the details of the spectral slopes and the proton yields for different trigger conditions. [S0556-2813(97)05805-6]

PACS number(s): 25.75.−q, 13.85.−t

*Present address: Lawrence Livermore National Laboratory, Livermore, California 94550.
†Present address: Columbia University, New York, New York 10027 and Nevis Laboratories, Irvington, New York 10533.
‡Present address: Radionics Software Applications Corp., Brookline, Massachusetts 02146.
§Present address: Ecole Polytechnique, F-91128 Palaiseau Cedex, France.
‖Present address: University of Tsukuba, Tsukuba, Ibaraki 305, Japan.
¶Present address: University of Tennessee, Knoxville, Tennessee 37996.
**Present address: Lawrence Berkeley Laboratory, Berkeley, California 94720.
††Present address: CERN, Geneva.
‡‡Present address: NITON, Bedford, Massachusetts 07130.
§§Present address: Institut fur Kernphysik, Frankfurt, D-6000, Germany.
‖‖Present address: Oak Ridge National Laboratory, Oak Ridge, Tennessee 37831.
¶¶Deceased.

I. INTRODUCTION

Relativistic heavy-ion beams from the Tandem-AGS complex at the Brookhaven National Laboratory have been used by several groups to study nuclear matter at high baryon density formed in heavy-ion collisions in the 10–15*A* GeV *c* range. Experiments with Si projectiles at 14.6*A* GeV/*c* have been performed in the last few years, and since 1992, a beam of Au at 11.7*A* GeV/*c* has also been available [1]. In a comprehensive experimental program, the E802 Collaboration [2] has measured the distributions of protons and produced particles over a broad range of rapidity (0.5–2.5 units) and transverse momentum (0.2–2.5 GeV/*c*) for a variety of projectile-target combinations ranging from $p+$Be to Si+Au [3–5] at 14.6*A* GeV/*c*.

Particle emission at target rapidities was not measured in the original E802 experiments. However, it was realized that such measurements are important for several reasons. It is desirable to have a complete measurement of baryon distributions in order to characterize the hot compressed system initially formed which, at the AGS energies, is expected to be baryon rich. In addition, the distribution of baryons emitted from the hot participant region is expected to be modified by rescattering and absorption in the target spectator matter. The breakup of the hot spectator can also contribute to baryon emission at target rapidities. Since protons observed at $\theta>90°$ cannot be produced in simple free nucleon-nucleon collisions, measurements at back angles serve to constrain and quantify such rescattering by and emission from the hot spectators and provide a test of the current theoretical models of relativistic heavy-ion collisions. For these reasons, an array of dual element scintillator telescopes (a phoswich [6] array) to measure target rapidity baryons was added to the E802 apparatus for the second generation experiment, E859.

In this paper, we present results for protons emitted in Si+Al,Cu,Au collisions at 14.6*A* GeV/*c* for pseudorapidities of $|\eta|\leq 0.76$ and kinetic energies of 40 MeV$\leq E_{\rm kin}\leq$225 MeV (280–690 MeV/*c* in momentum). For the Si+Au system, we also report deuteron results. These Si beam data were obtained during dedicated running periods in 1991 and 1992. The silicon program was concluded in April 1992 and in this paper we report the final results of our study using this projectile. At the conclusion of the silicon program, a Au beam at 11.7*A* GeV/*c* was commissioned and briefly made available for experimental use. Although the E859 phoswich array was not optimized for the particle multiplicities in Au+Au collisions, it was possible to make a first set of measurements for Au+Au by reconfiguring the array. The results of those measurements are also reported here. Since then, we have made extensive measurements of baryon emission from Au+Au at target rapidities, as part of experiment E866, using a larger phoswich array with segmentation appropriate for the multiplicities in Au collisions. Those results will be published in the future. The first Au+Au measurements reported here provide a direct link between the measurements of target rapidity protons made using the E859 phoswich array and the more recent measurements using the new E866 array.

The present measurements, along with results for $p+$Au from the literature, provide us with the systematics on baryon emission at target rapidities as a function of target-projectile combination and the centrality of the heavy-ion collisions. We also make comparisons of our results with the predictions of two current models ARC and RQMD.

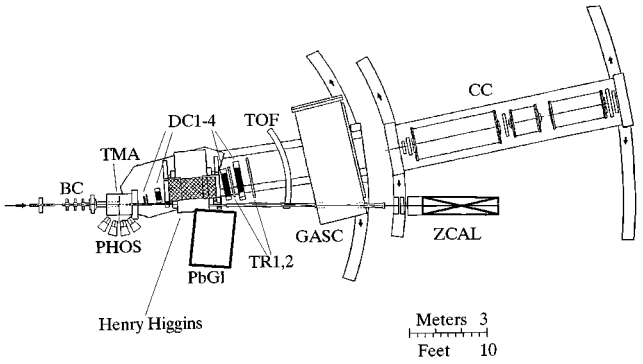

FIG. 1. View from above the E859 apparatus.

II. EXPERIMENTAL DETAILS

The present measurements were made as part of the study of relativistic heavy-ion collisions at the AGS at Brookhaven National Laboratory by the E802 Collaboration in experiments E859 and E866.

A. Phoswich array

The E802 experimental setup has been described in detail by Abbott *et al.* [2]. As mentioned above, in experiment E859, a phoswich array covering the angular range 50°–130° [pseudorapidity $|\eta|\leq 0.76$, where $\eta\equiv-\ln(\tan\theta/2)$] was added to the E802 setup for measuring charged particle emission at target rapidities. The E859 setup, including the phoswich array, is shown in Fig. 1.

Details on the phoswich array and its performance have been published elsewhere [7]. The array consisted of 42 ΔE-E phoswich scintillator telescopes, each telescope read out with a single photomultiplier tube. The ΔE and time-of-flight information was provided by 5 mm of BC412 (''fast''), a scintillating plastic with short rise and decay times ($t_{\rm rise}=1.0$ ns, $t_{\rm decay}=3.3$ ns). The E section was 26 cm of BC444 (''slow''), a scintillating plastic with a relatively long rise time and a very long decay time ($t_{\rm rise}=19.5$ ns, $t_{\rm decay}=260$ ns). The array consisted of modules of two different solid angles, with the smaller modules (24 total) being used at the more forward angles where the hit density was highest. The large modules (18 total) have the shape of truncated pyramids with the front face being 8.53×8.53 cm^2 and the back being 12.19×12.19 cm^2. The smaller modules were fabricated by quartering large modules along the longitudinal axis, producing four identical small module from each large module. These four small modules were then repackaged, each with its own photomultiplier tube, into the form of the large modules so that a common mount could be used for both large and small modules. The detectors were mounted approximately 65 cm from the target and the array subtended a polar angular and azimuthal range of 50.2°–129.8° and $\Delta\phi\simeq 24°$, respectively, on the side of the beam opposite to the E802 spectrometer.

The use of two different analog-to-digital converter (ADC) gates (60 and 220 ns in duration) on the single photomultiplier tube (PMT) signal permits the unfolding of the two signal components from the fast and slow scintillators. The ΔE-E and time-of-flight information allow the separation of ''neutrals'' (gammas, neutrons, and charged particles not passing through the fast plastic), charged pions, protons, deuterons, and tritons over a broad range of kinetic energy (up to 250 MeV for protons). The response of both small and large phoswich modules to protons and deuterons of known incident energies was measured at the Indiana University Cyclotron Facility as described in Ref. [7].

The lower-energy threshold for proton detection (25–45 MeV) is mainly determined by the energy loss in the target. Unambiguous determination of the proton energy is possible for energies up to 110–220 MeV, depending upon the laboratory angle of the measurement.

B. Targets

The thicknesses of the Al and Cu targets were 817 and 1440 mg/cm^2, respectively, which corresponded to 3% of an interaction length for the Si beam. The thickness of the Au target was 944 mg/cm^2 or 1% of an interaction length for the Si beam and 1.5% for the Au beam. Target-out runs were performed to determine background contributions for all systems. Target-out contributions have very little effect on the particle spectra and primarily affect the cross section normalization.

C. Hardware triggers

1. Si beam runs

To select central events with Si projectiles, we used the standard E802 Target Multiplicity Array (TMA) trigger [4]. This trigger was made by putting a hardware cut on the charged particle multiplicity measured by the Target Multiplicity Array [2] corresponding to the upper 7% of the measured multiplicity distribution. Minimum bias data were acquired using an interaction trigger, INT, defined for the E802 apparatus in Ref. [4]. Since not every INT trigger produced data in the phoswich array, we defined a new hardware trigger, PHOS, which was simply INT and at least one hit (an OR of all discriminators) in the phoswich array.

2. Au beam runs

For Au+Au collisions, we used hardware triggers that were based on the kinetic energy measured in the Zero Degree Calorimeter (ZCAL) [2]. The central collision trigger was made by requiring that the ZCAL energy be below a threshold which selected the most central 4% of all interactions. The minimum bias trigger selected all events below a threshold that was set just below the beam energy peak in the ZCAL spectrum.

The use of two different methods to select central events deserves a comment. Multiplicity and ZCAL energy are inversely related, in general. The most central events have the highest multiplicity, but have the fewest projectile spectators, thus giving the lowest ZCAL energy. The distribution of multiplicity versus ZCAL energy has significant width, arising from fluctuations in the two quantities and from instrumental resolution. However, in the case of Si+Al collisions, E802 has reported that a TMA trigger representing the upper $7a$ software cut with ZCAL energy $\leqslant 80$ GeV gives the same results on particle production at midrapidity [4]. For the most central Si+Au collisions, the ZCAL energy cannot give a good trigger, since the silicon nucleus is completely occluded by the Au nucleus for a range of impact parameters and the ZCAL energy stays nearly constant. For Au+Au in the present study, the TMA could not be used as a central trigger as it was not designed for the high multiplicities involved and a ZCAL cut was used, instead.

D. Corrections, efficiencies, and uncertainties

The data have been corrected for the geometrical acceptance, energy loss, and multiple scattering in the target and particle identification efficiency (protons which scatter out of the module before stopping may not be identified as protons). These corrections were determined by means of Monte Carlo simulations [7] using the GEANT code [8]. Corrections were also made, as a function of angle and kinetic energy, for background arising from sources such as multiple hits, target-out contributions, and pions or protons that punch through the detector without stopping. At the more backward angles, particle identification (PID) is possible for the full dynamic range of the detector modules (over 200 MeV). At more forward angles, the hit density effectively limits unambiguous PID for protons to approximately 110 MeV mainly because in ΔE-E space multiple hits from minimum ionizing particles obscure the proton band at kinetic energies higher than 110 MeV.

In this paper, we report particle yields as yields per event trigger. As stated above, the minimum bias data from Si beam runs were for PHOS events which were INT events in which there was at least one hit in the PHOS array. The particle yields per PHOS event measured in these runs were converted to the physically more meaningful yields per INT trigger using the observed ratio of PHOS to INT events.

Only statistical uncertainties are shown in the various figures in Sec. III which report the results of these measurements. Systematic errors in the normalization of the kinetic energy spectra and the particle yields obtained in Sec. III by integrating the spectra over the measured energy interval are estimated to be $\pm 15\%$, in general. A major fraction of this uncertainty ($\leqslant 10\%$ for most data points) is associated with the phoswich acceptance correction (based on Monte Carlo calculations) for particles of different energies and emission angles. The phoswich energy calibration contributes 3–4 %. For the measurements at laboratory angles close to 90° the uncertainty from acceptance correction is larger (because of the amount of matter the particles have to traverse in the target and in the particular target mount used in these experiments) and an overall uncertainty of $\pm(20-25)\%$ must be assigned to these points. The irregularity in the points at η near 0 in the pseudurapidity density distributions for the Au target in Fig. 9 is ascribed to this higher systematic uncertainty in the acceptance correction.

III. RESULTS AND DISCUSSION

A. Kinetic energy spectra and pseudorapidity distributions

In Fig. 2, the measured proton momentum density distri-

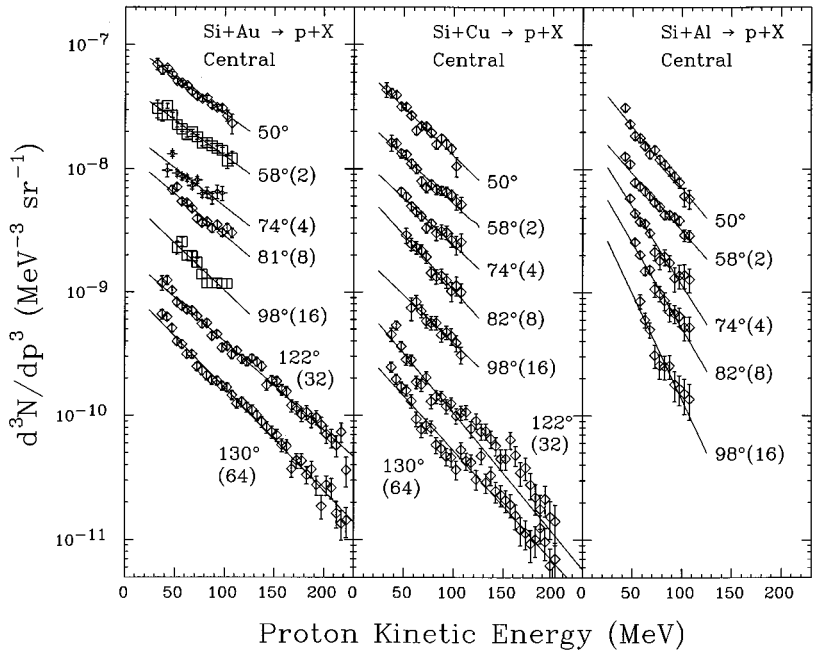

FIG. 2. Momentum density distribution d^3N/dp^3 plotted at fixed angles as a function of the kinetic energy of protons from central Si+Au, Si+Cu, and Si+Al collisions. Solid lines represent exponential fits made in the kinetic energy range 50 MeV $\leqslant E_{\rm kin} \leqslant$ 110 MeV. Starting with the second spectrum from the top, the ordinate in each succeeding spectrum has been divided by a factor of 2 for clarity of presentation.

butions d^3N/dp^3 are plotted as a function of kinetic energy for central Si+Al, Si+Cu, and Si+Au collisions. These data include all the laboratory angles measured by the array. As mentioned above, the spectra at the forward angles are limited to kinetic energies less than 110 MeV, and at the back angles they extend up to 200 MeV. For the Si+Al reaction, the spectra at the most backward angles had inadequate statistics and and these angles are not included in Fig. 2. For all three targets, in general, the spectra become steeper with increasing laboratory angle. Figure 2 also shows exponential fits to the spectra which are discussed below. As one moves back in angle, the proton yield changes relatively little in the angular range $50° < \theta < 90°$, but decreases rapidly in the backward hemisphere.

In Fig. 3, we compare the proton spectra from the present work with that measured previously by the E802 spectrometer [4] for central collisions at 50°. The spectra measured by the two detectors overlap over a small range in energy. However, the systematic uncertainties in both the spectrometer and phoswich data are greatest in the overlap region: Multiple scattering severely limits the proton measurement in the spectrometer below 150 MeV, while the multiple hit background limits the proton PID in the phoswich array above 110 MeV at these angles. In view of this, the spectra measured by the two detectors are not inconsistent. The comparison in Fig. 3 also shows that the spectra are not well described by a single exponential shape over the entire energy range, but consist of at least two regions with different slopes. Proton spectra from $p+A$ collisions have previously been shown to behave in a similar manner, with smaller inverse slopes at lower kinetic energies [9].

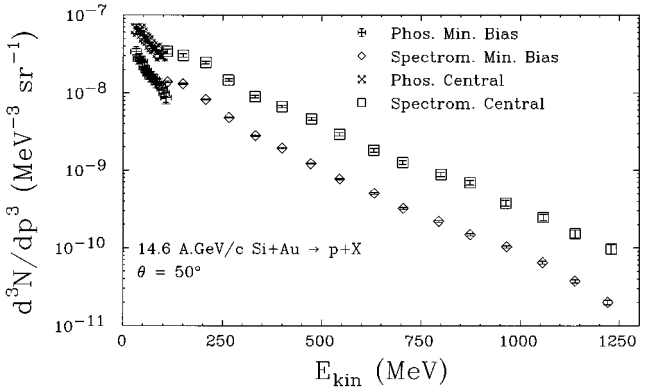

FIG. 3. Comparison of proton spectra at 50° measured by the phoswich array and the E802 spectrometer.

In Fig. 4 proton spectra for minimum bias Si+Al and Si+Au are shown. For Si+Al, the minimum bias statistics are satisfactory up to the largest angle measured (130°). The general features of the minimum bias spectra are very similar to those from central collisions shown in Fig. 2. As in the case of central collisions, the spectra get steeper and the yield decreases steadily with angle in the backward hemisphere.

Figure 5 shows proton spectra for minimum bias and central collisions for the reaction Au+Au. As discussed in Sec. II, the segmentation of the E859 phoswich array was inadequate for use at the forward angles for central Au+Au collisions. Proton spectra at larger angles given in Fig. 5 were measured by moving the subarray of 24 small phoswich modules to different angles. Again, the spectra become steeper with angle and the yield decreases with angle in the backward hemisphere.

As pointed out above, we characterize the spectra by fitting them to exponential distributions in kinetic energy $[d^3N/dp^3 = C\ \exp(-E_{\rm kin}/B)]$. We restrict the fits to the energy interval 50–110 MeV for the following reasons. The measured spectra at the forward angles do not extend beyond 110 MeV. The backward angle spectra extending up to 200 MeV are not well described by a single exponential and, in

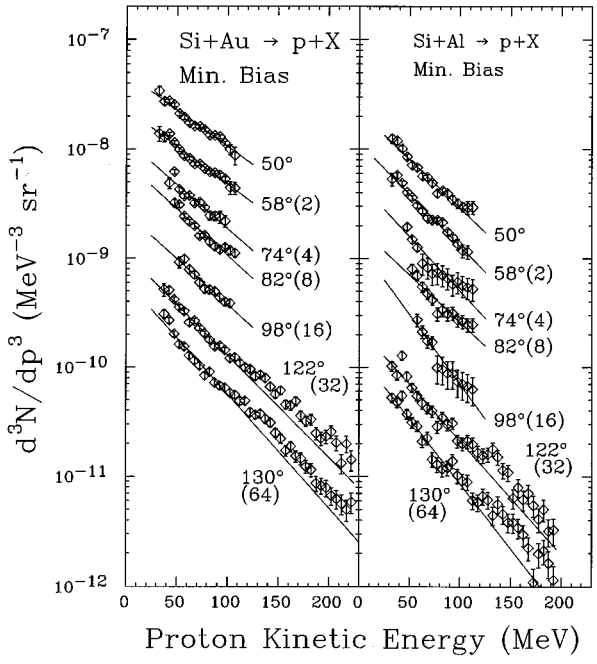

FIG. 4. Same as Fig. 2, for minimum bias Si+Au and Si+Al.

addition, sometimes show a kink at around 110 MeV probably due to background contamination not completely removed. As indicated by the solid lines in Figs. 2, 4, and 5, the spectra are well described by single exponentials in the energy range 50–110 MeV.

In Fig. 6, we show the inverse slopes obtained from the exponential fits. The inverse slopes vary from 40 to 80 MeV,

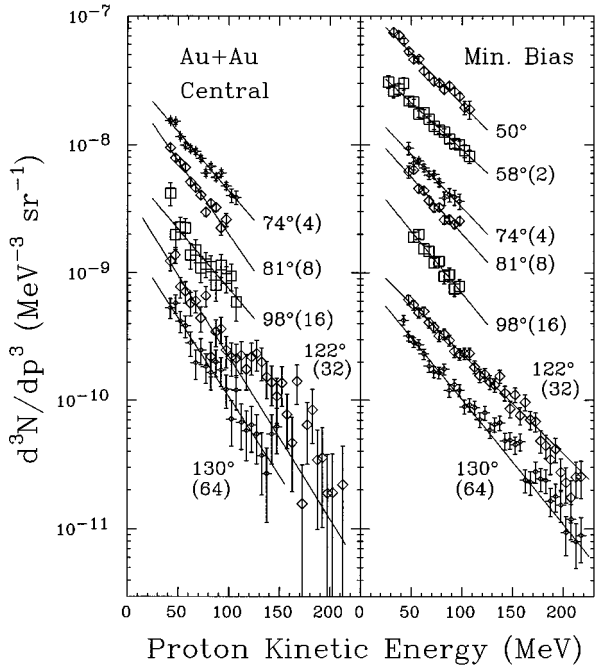

FIG. 5. Same as Fig. 2, for central and minimum bias Au+Au.

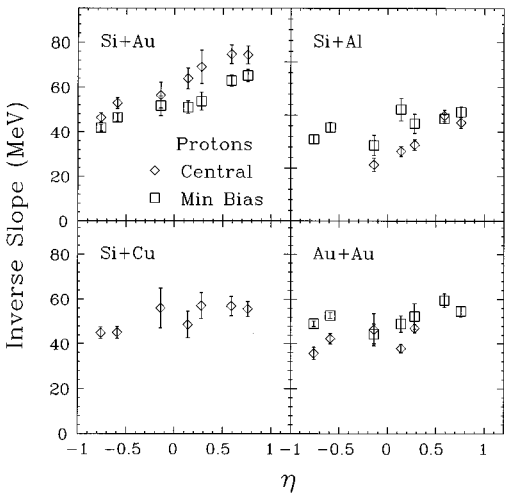

FIG. 6. Inverse slope parameters for proton spectra from exponential fits in the kinetic energy range 50–110 MeV.

generally increasing with increasing pseudorapidity. These slopes represent appreciable mean kinetic energies for protons being emitted at such large angles. The inverse slopes for Si+Au are about 20% greater for central collisions than for minimum bias collisions. In contrast, for Si+Al and Au+Au the inverse slopes for minimum bias collisions are slightly higher. However, the most remarkable feature is the qualitative similarity of the results for these four different systems and extremes in event characterization (minimum bias and central).

The deuteron kinetic energy spectra for Si+Au are shown in Fig. 7. As in the case of protons, the deuteron spectra get steeper and the yields decrease for increasing laboratory angles. We have fitted the deuteron spectra to an exponential distribution over the energy range 70–130 MeV. The fits are shown in Fig. 7. The deuteron slope parameters are given in Fig. 8. The inverse slopes are nearly constant except for the two most forward angles. The values for central triggers are slightly larger than those for minimum bias. At back angles, the deuteron inverse slopes are slightly smaller than the proton values.

In order to quantify the particle yields from these measurements, we have integrated the proton spectra over the kinetic energy interval $50 \leqslant E_{\mathrm{kin}} \leqslant 110$ MeV and the deuteron spectra over the interval $70 \leqslant E_{\mathrm{kin}} \leqslant 130$ MeV. The resulting proton pseudorapidity densities are shown in Fig. 9 for all systems. The deuteron pseudorapidity densities for Si+Au are shown in Fig. 10. These $dN/d\eta$ values are obtained by summing the measured spectra in the respective kinetic energy intervals directly and therefore do not depend on the fit results. Because the spectra are not exponential over the entire energy range, there is no reliable method to allow extrapolation of the spectra outside the measured interval to obtain total $dN/d\eta$. We therefore do not extrapolate the yields outside the chosen energy intervals. To stress that the *integration* is done over a limited energy range, we denote the resulting values throughout by the symbol $dN(E_{\mathrm{lim}})/d\eta$. We estimate that these values represent about 20–30 % of the proton or deuteron yield at each angle which is a large enough measured fraction to test the success of

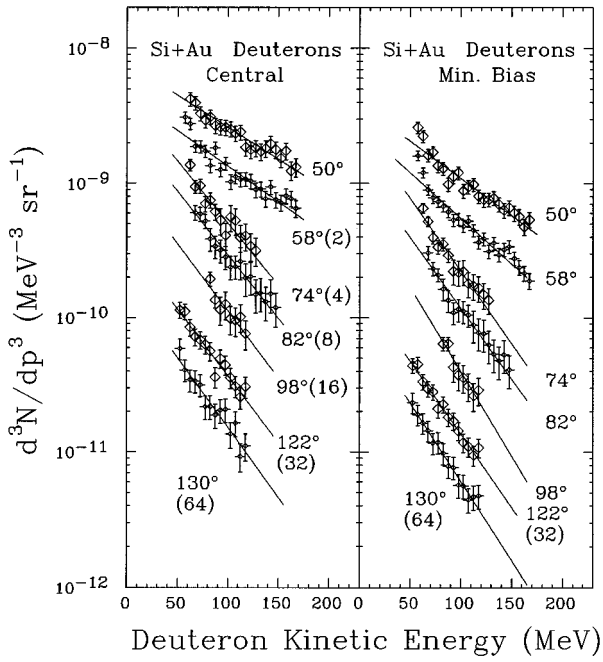

FIG. 7. Momentum density distribution d^3N/dp^3 plotted at fixed angles as a function of the kinetic energy of deuterons from minimum bias and central Si+Au collisions. See caption for Fig. 2 regarding normalization of the spectra.

reaction models in describing the emission of baryons at target rapidities. Thus they constitute a well-defined data set to which predictions of models can be compared after applying appropriate experimental filters (see Sec IV).

B. Comparison of $dN(E_{\rm lim})/d\eta$ distributions for different reactions

It is seen from Fig. 9 that the absolute yield of protons per collision in the selected energy range increases as the centrality is increased for Si+Au and Si+Al collisions. Figure 10 shows that for Si+Au the deuteron yield is also higher in central than in minimum bias collisions. In contrast, for the Au+Au system, the yield of protons per collision in the selected energy interval (Fig. 9) is very similar for both central and minimum bias collisions. The $dN(E_{\rm lim})/d\eta$ distributions for the different systems and triggers have very similar shapes as emphasized by the logarithmic scale in Fig. 9. All

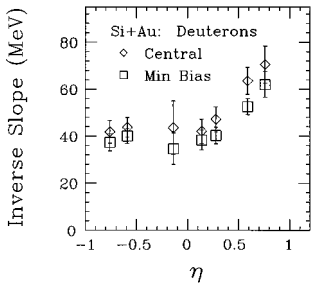

FIG. 8. Inverse slope parameters for Si+Au deuteron spectra from exponential fits in the kinetic energy range 70–130 MeV.

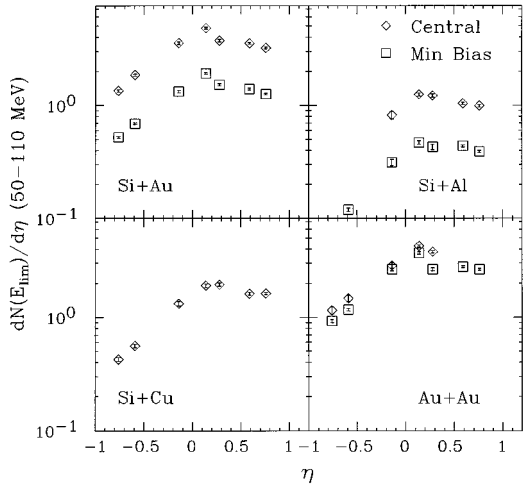

FIG. 9. $dN(E_{\rm lim})/d\eta$ distributions of protons with kinetic energy in the range 50 MeV$\leqslant E_{\rm kin}\leqslant$110 MeV.

the $dN(E_{\rm lim})/d\eta$ distributions clearly peak above $\eta=0$. For the proton kinetic energy interval 50–110 MeV, our most forward point in the distributions in Fig. 9 corresponds to a mean rapidity of 0.2. The proton rapidity density distribution dN/dy is known to decrease rapidly for $y\geqslant 0.5$ [4]. The location of the expected peak in the total $dN/d\eta$ distribution cannot be determined from the present data alone since the hard component which would dominate at the forward angles is not included.

It is interesting to compare our results for proton emission in nucleus-nucleus collisions with those for proton-nucleus collisions reported in the literature. Abbott *et al.* [5] have reported results of $p+A$ studies at 14.5 GeV using the E802 spectrometer at angles forward of 50°. The proton kinetic energy spectra from their work (invariant cross section versus proton kinetic energy) did not extend below 200 MeV in kinetic energy. Furthermore, it was observed that a single exponential did not fit these spectra satisfactorily over the full measured energy range (200–2500 MeV). We fit the region below 1 GeV in the proton spectra where a single exponential form is appropriate and used the fitted parameters to calculate $dN(E_{\rm lim})/d\eta$ of protons in the (unmeasured) kinetic energy interval 50 MeV$\leqslant E_{\rm kin}\leqslant$110 MeV for

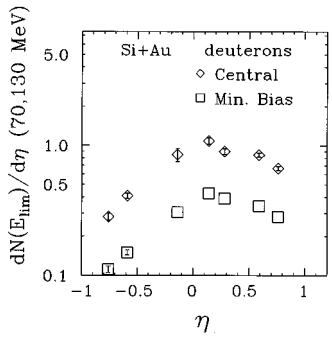

FIG. 10. $dN(E_{\rm lim})/d\eta$ distributions of deuterons with kinetic energy in the range 70 MeV$\leqslant E_{\rm kin}\leqslant$130 MeV from Si+Au collisions.

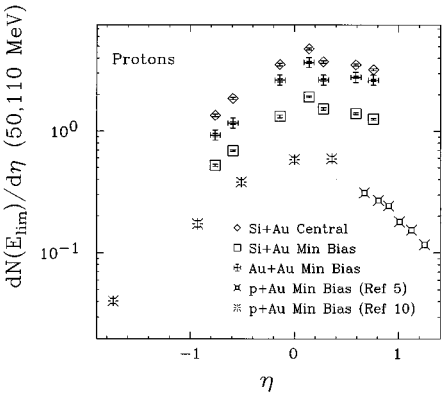

FIG. 11. Comparison of $A+A$ and $p+A$ $dN(E_{\rm lim})/d\eta$ values.

comparison with the phoswich data. The results are shown in Fig. 11.

Particle production in proton nucleus collisions at high energies has been reviewed by Frederikson *et al.* [10]. It has been shown that proton spectra at back angles are characterized by slope parameters which depend only weakly on target mass and beam momentum [9–11]. Bayukov *et al.* [11] have reported proton spectra from the reactions of 400 GeV protons on targets ranging from Li to Ta under minimum bias conditions over an angular range very similar to our phoswich measurements. They showed that the proton spectra (expressed as invariant cross section per nucleon) at 160° from $p+$C and $p+$Cu at 8 and 400 GeV were indistinguishable in shape and magnitude. Fitting the proton spectra from $p+A$ at 400 GeV reported by Bayukov *et al.* [11] the same way as the phoswich data from our Si+Au measurements and using the smooth target dependence of the resulting $dN(E_{\rm lim})/d\eta$ values, we have obtained $dN(E_{\rm lim})/d\eta$ for $p+$Au by extrapolation. (The measurements of Bayukov *et al.* included $p+$Ta and therefore the extrapolation to $p+$Au amounted to only a few percent.) These results, also shown in Fig. 11, match well with the extrapolation of the forward angle measurements by E802 experiment for $p+$Au at 14.6 GeV/c.

The $dN(E_{\rm lim})/d\eta$ distributions for minimum bias Au+Au and Si+Au are also replotted in Fig. 11 for comparison. It is noteworthy that all the $dN(E_{\rm lim})/d\eta$ distributions plotted in Fig. 11 have very similar shapes. If we scale up the $p+$Au distribution by factors of 2.4 and 6.0, respectively, we can match the Si+Au minimum bias and central results reasonably well. These scale factors do not seem to be related in any simple way to the relative numbers of participants and spectators in the different cases. For comparison, the total number of participants (target spectators) is calculated on the basis of the Fritiof model to be 5(193), 35(174), 101(124), and 102(146) for $p+$Au minimum bias, Si+Au minimum bias, and Si+Au central and minimum bias Au+Au collisions, respectively [12].

Rescattering and absorption of participant protons in the target spectator matter and emission of protons by heated spectator matter are all factors which would depend on the relative size of target and projectile and on the collision centrality. These factors would be expected to affect the shape of the angular distribution of protons at target rapidities. The

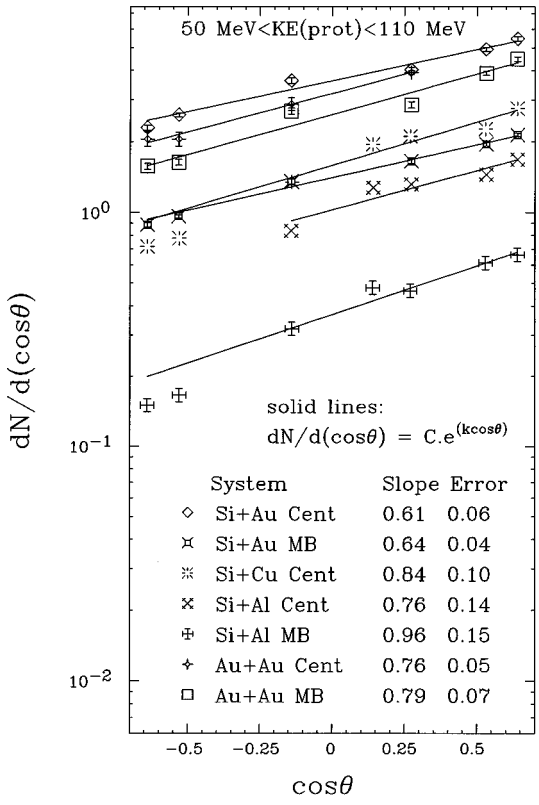

FIG. 12. Angular distributions of protons from various systems measured in this work. Exponential fits are also shown (see text).

similarity in the shape of the distributions suggests that the protons emitted at target rapidities from the different reactions have a common source. Since we are focusing on relatively low energy protons (and not including the harder component which is evident in Fig. 3), the most important mechanism may be the emission from or breakup of the target spectators, with rescattering of participant protons playing a lesser role.

Albrecht *et al.* [13] observed that the angular distributions of slow protons ($30 \leqslant E_{\rm kin} \leqslant 400$) from oxygen- and proton-induced reactions at 60A and 200A GeV are well represented by $dN/d\cos(\theta) = C\exp(k\cos\theta)$. The slopes of the distributions decreased with increasing target-projectile asymmetry and also with increasing impact parameter. It has been suggested that smaller slopes (flatter angular distributions) in the case of the asymmetric systems may be the result of greater rescattering. Figure 12 displays our proton angular distributions in this form. These data show an approximate trend of the type seen by Albrecht *et al.* in the angular distributions. Thus, the most asymmetric system Si+Au has the smallest slope and the more symmetric systems, in general, have larger slopes. However, it is difficult to relate dependences of this type quantitatively to contributions from rescattering or target spectator breakup.

C. Centrality dependence

The centrality dependence of target rapidity baryon emission can be studied in more detail using the information provided by the E802 Zero-Degree Calorimeter (ZCAL) which allows impact parameter selection on the basis of the energy

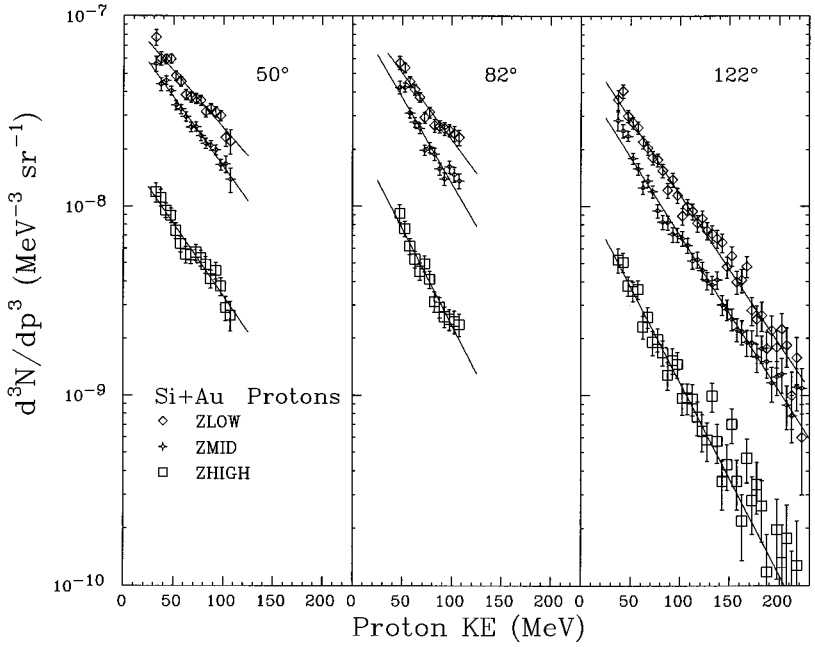

FIG. 13. Proton momentum density distributions from Si+Au for three cuts in ZCAL energy.

remaining in projectile fragments [2]. We have analyzed our Si+Au proton and deuteron data by dividing the events into three ZCAL energy bins $Z_{\rm low}=0\leqslant E_{\rm ZCAL}\leqslant 60$ GeV, $Z_{\rm mid}=60$ GeV$\leqslant E_{\rm ZCAL}\leqslant 250$ GeV, and $Z_{\rm high}=250$ GeV$\leqslant E_{\rm ZCAL}\leqslant 420$ GeV. On the basis of a simple calculation of overlapping spheres, these $E_{\rm ZCAL}$ cuts correspond to the impact parameter intervals 0.0–4.7, 4.7–7.9, and 7.9–10.6 fm, respectively.

In Fig. 13, we show proton kinetic energy spectra for Si+Au at three angles for the three ZCAL cuts. The features of these spectra are very similar to those already displayed in Fig. 2. The spectra for each bin get steeper with angle. The spectra for the two lowest ZCAL bins are very similar in both slope and magnitude, presumably reflecting the relatively small change in the numbers of participants (spectators) between these two bins. In Fig. 14, we plot the inverse slope parameters and $dN(E_{\rm lim})/d\eta$ values as a function of pseudorapidity. As expected, from the similarity of the distributions for central (TMA) and minimum bias triggers presented earlier, the proton pseudorapidity distributions for the three impact parameter intervals in Fig. 14 are very similar in shape. This is underscored by the nearly constant values of the ratios of $dN(E_{\rm lim})/d\eta$ values plotted in Fig. 15.

Figure 16 displays the deuteron/proton ratios for the three impact parameter intervals as a function of pseudorapidity. The ratio shows little dependence on η or ZCAL cut. The mean values are 0.29, 0.29, and 0.26 for the low, middle, and high ZCAL cuts, respectively.

IV. COMPARISON WITH MODELS

The transport-theoretical models RQMD [14] and ARC [15] have had considerable success in explaining a number of experimental measurements from relativistic heavy-ion collisions at midrapidities [11,12]. However, the models have remained largely untested at target rapidities. In this section, we present comparisons of the experimental results at target rapidities with those calculated using these two models. We emphasize the Si+Au system here for which comparisons of measured and calculated proton spectra and yield distributions are presented in detail. For Au+Au and p+Au, the comparisons are limited to yield distributions.

A. Si+Au

RQMD version 1.07 and ARC version 1.15 were used. In each case, we have started with a minimum bias distribution of events and applied suitable cuts to select events corresponding to our hardware triggers and geometric acceptance. To correspond to the minimum bias trigger, we started with a pool of events with impact parameter $\leqslant 11$ fm and selected events in which the projectile lost at least one proton in the interaction (as counted by the number of beam momentum protons in the angular interval defined by the bulls-eye counter in the apparatus [2]). A subset of these were chosen as central events corresponding to the upper 7% of the charged particle multiplicity distribution, where the multiplicity was given by the number of charged particles ac-

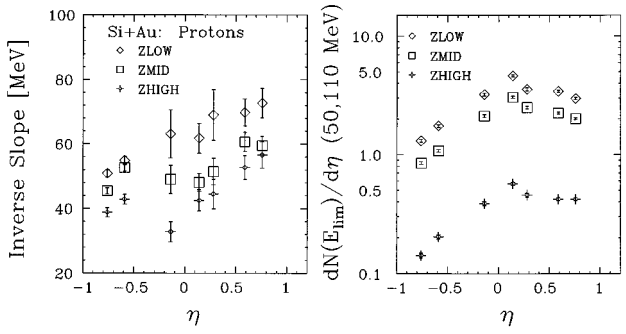

FIG. 14. Inverse slope parameters and $dN(E_{\rm lim})/d\eta$ distributions for protons from Si+Au for the three ZCAL cuts.

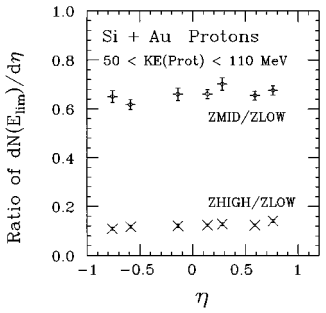

FIG. 15. Ratios of proton $dN(E_{\rm lim})/d\eta$ values for for Si+Au for the three cuts in ZCAL energy.

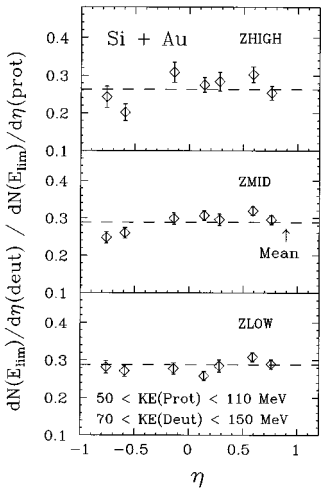

FIG. 16. Deuteron/proton ratios for Si+Au for the three cuts in ZCAL energy.

cepted by a filter that imposed the geometry of the Target Multiplicity Array and also applied a minimum kinetic energy requirement of 25 MeV for each particle. The model events were analyzed in the same manner as the experimental data.

In Fig. 17, we compare the experimental proton momentum density distributions for central Si+Au events at 50° and 130° with those given by the two models. The calculated spectra from the two models are very similar to each other. At 50°, both models give spectra whose slopes are close to the experimental slopes, but the model cross sections are too high by a factor of 2. At 130°, the model spectra are much steeper than the experimental ones. However, the cross sections appear to be closer to the data. The model spectra were fit to an exponential over the kinetic energy interval 50–110 MeV, and the inverse slope parameters from the fits are compared to the experimental values in Fig. 18. Except for central collisions at the most forward angles, the inverse slopes of the model spectra are considerably smaller than the experimental values. Thus for Si+Au, both the models, in general, predict spectra which are significantly softer than the data.

The calculated $dN(E_{\rm lim})/d\eta$ values for Si+Au are compared to the measurements in Fig. 19. At the forward angles measured by the phoswich array, both RQMD and ARC overestimate the yield of protons in the kinetic energy interval of 50–110 MeV, but come closer to the experimental data at backward angles. In this context, it should be remembered that both RQMD and ARC do not produce clusters. Therefore, the contributions from deuteron and heavier species should be added to the proton results before a comparison is made. However, since we integrate the spectra only over a limited energy interval, we actually do not include the deuteron contribution in the data plotted in Fig. 18, but note that the deuteron-to-proton ratio is close to 0.3 at all angles as can be seen from Fig. 16. If a deuteron contribution of this magnitude is added to the measured proton yields, the discrepancy between the measurements and the model values would be significantly reduced, bringing the two sets of values within reasonable agreement in the backward hemisphere. In summary, the models give a fairly consistent representation of the proton yields from Si+Au in the energy range of our

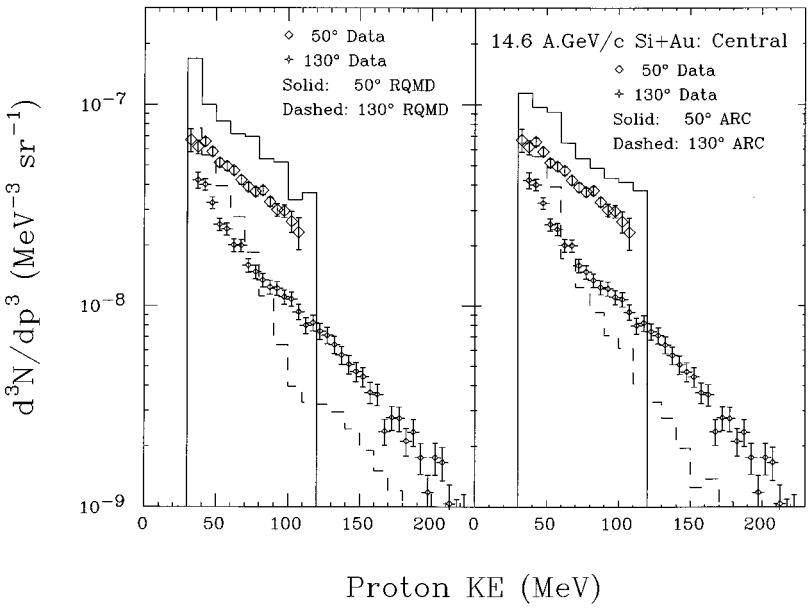

FIG. 17. Comparison of experimental proton spectra for central Si+Au events with those calculated by RQMD and ARC models.

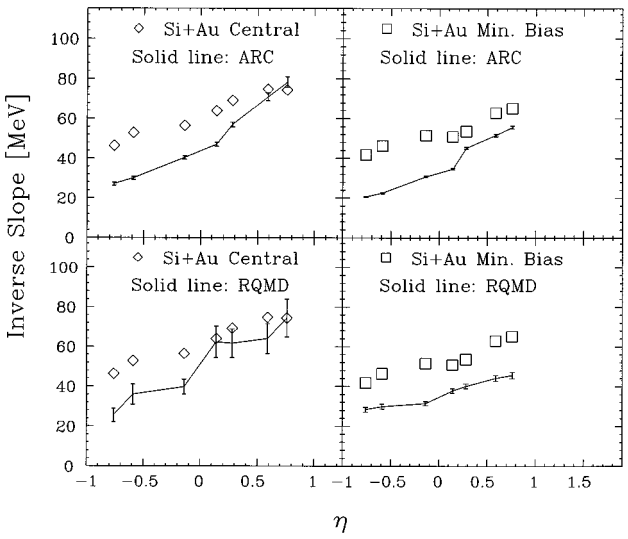

FIG. 18. Comparison of experimental Si+Au proton slope parameters with both RQMD and ARC calculations.

measurements, especially at back angles, but do a rather poor job on the spectral shapes.

B. Au+Au

In this case, a pool of model events with impact parameter $\leqslant 14$ fm was used as minimum bias events. To correspond to the ZCAL central trigger used experimentally, the most central 4% of events were selected by requiring that the calculated energy incident in the Zero Degree Calorimeter aperture was below a threshold value. Figure 20 shows a comparison of the experimental data with the results from the model simulations. The inverse slopes, shown in the left-hand panel, change more rapidly with angle than the experimental values except for RQMD minimum bias events. The $dN(E_{\rm lim})/d\eta$ values are shown in the right-hand panel. In both models, the minimum bias values are higher than the central values, although in ARC the central and minimum bias

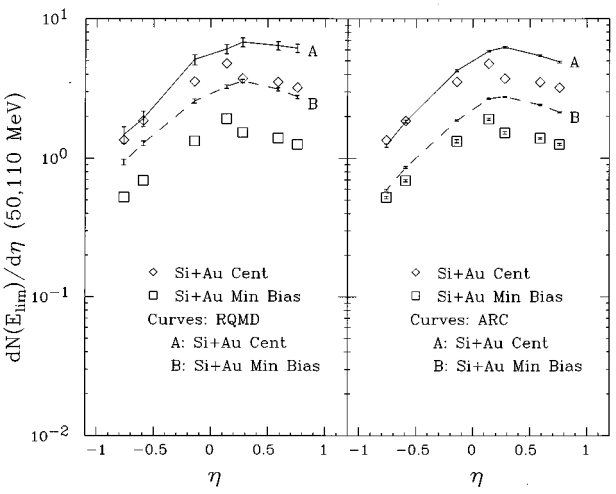

FIG. 19. Comparison of experimental Si+Au proton $dN(E_{\rm lim})/d\eta$ distributions with both RQMD and ARC calculations.

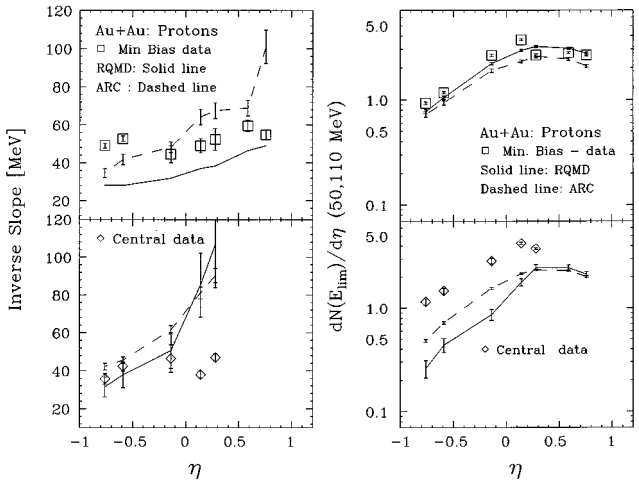

FIG. 20. Comparison of experimental Au+Au proton slope parameters and proton $dN(E_{\rm lim})/d\eta$ distributions with both RQMD and ARC calculations.

results are very close to each other as in the experiment. The calculated values are close to the measurements for minimum bias events, but significantly lower in the case of central events. The inclusion of deuterons in the experimental results will increase the disagreement in all cases. For central events the experimental $dN(E_{\rm lim})/d\eta$ values are 2–3 times larger than the ARC values and 2–5 times larger than the RQMD values. Thus both ARC and RQMD predict, in general, harder momentum density distributions and lower yields (in the kinetic energy range 50–100 MeV) than the experimental values for protons from Au+Au at target rapidities. The direction of the disagreement for Au+Au is in general opposite to that in the case of Si+Au.

V. SUMMARY AND CONCLUSIONS

In summary, we report measurements of proton emission at target rapidities for minimum bias and central collisions of 14.6A GeV/c ^{28}Si with Al, Cu, and Au nuclei as well as minimum bias and central collisions of 11.7A GeV/c ^{197}Au with Au nuclei. Deuteron results are also reported for Si+Au. The results include the inverse slopes of proton spectra and pseudorapidity density distributions in the kinetic energy range 50 MeV$\leqslant E_{\rm kin} \leqslant$110 MeV. The inverse slopes generally increase with increasing pseudorapidity for the various systems. The $dN(E_{\rm lim})/d\eta$ values for $A+A$ collisions are compared to those for protons from $p+$Au in the literature. All pseudorapidity distributions have very similar shapes. There are only small differences among the values of the slopes of proton angular distributions from asymmetric and symmetric systems when fitted as exponentials in cos θ. While the contributions from target breakup or rescattering of participant protons by the target spectator may be expected to depend on the relative sizes of the target and projectile and the centrality of the collision, these variables seem to have only a small effect on the shape of the measured proton distributions at target rapidities. The nucleon-nucleon collision models ARC and RQMD generally reproduce this feature, but there are significant disparities in the details of the spectral slopes and the proton yields.

ACKNOWLEDGMENTS

The authors would like to thank the Tandem and AGS staff at Brookhaven for providing the silicon and gold beams. We are indebted to G. Peilert for the RQMD calculations and discussions and to T. Schlagel for the ARC calculations and discussions. This work has been supported by the U.S. Department of Energy under contracts with ANL (W-31-109-ENG-38), BNL (DE-AC02-76CH00016), Columbia University (DE-FG02-86-ER40281), LLNL (W-7405-ENG-48), MIT (DE-AC02-76ER03069), UC Riverside (DE-FG03-86ER40271), by NASA (NGR-05-003-513), under contract with the University of California, by KOSEF (951-0202-032-2) in Korea under contract with Yonsei University, and by the U.S.-Japan High Energy Physics Collaboration Treaty.

[1] See, e.g., Proceedings of Quark Matter '91 [Nucl. Phys. **A544**, 1c (1992)]; Quark Matter '93 [*ibid.* **A566**, 1c (1994)]; Quark Matter '95 [*ibid.* **A590**, 1c (1995)].

[2] T. Abbott *et al.*, Nucl. Instrum. Methods Phys. Res. A **290**, 41 (1990).

[3] T. Abbott *et al.*, Phys. Rev. Lett. **64**, 847 (1990); Phys. Rev. Lett. **66**, 1567 (1991).

[4] E802 Collaboration, T. Abbott *et al.*, Phys. Rev. C **50**, 1024 (1994).

[5] E802 Collaboration, T. Abbott *et al.*, Phys. Rev. D **45**, 3906 (1992).

[6] D. H. Wilkinson, Rev. Sci. Instrum. **23**, 414 (1952); A. Baden *et al.*, Nucl. Instrum. Methods Phys. Res. A **203**, 189 (1982).

[7] J. B. Costales, H. C. Britt, M. N. Namboodiri, T. C. Sangster, J. H. Thomas, and H. E. Wegner, Nucl. Instrum. Methods Phys. Res. A **330**, 183 (1993).

[8] Rene Brun *et al.*, GEANT 3 Users' Guide, Report No. DD/EE/84-1, CERN, 1987.

[9] T.-A. Shibata *et al.*, Nucl. Phys. **A408**, 525 (1983); H. En'yo *et al.*, Phys. Lett. B **195**, 1 (1985).

[10] S. Fredriksson, G. Eilam, G. Berlad, and L. Bergstrom, Phys. Rep. **144**, 187 (1987).

[11] Y. D. Bayukov, V. I. Efremenko, S. Frankel, W. Frati, M. Gazzaly, G. A. Leksin, N. A. Nikiforov, C. F. Pedrisat, V. I. Tchistilin, and Y. M. Zaitsev, Phys. Rev. C **20**, 764 (1979).

[12] C. G. Parsons, Ph.D. thesis, Massachusetts Institute of Technology, 1992.

[13] R. Albrecht *et al.*, Phys. Lett. B **307**, 269 (1993).

[14] H. Sorge, H. Stocker, and W. Greiner, Ann. Phys. (N.Y.) **192**, 266 (1989); H. Sorge, Nucl. Phys. **A498**, 567c (1989).

[15] Y. Pang, T. J. Schlagel, and S. H. Kahana, Phys. Rev. Lett. **68**, 2743 (1992); T. J. Schlagel, Y. Pangand, and S. H. Kahana, Phys. Rev. Lett. **69**, 3290 (1992).